Peptide–Silica Hybrid Networks: Biomimetic Control of Network Mechanical Behavior

Aysegul Altunbas,[†] Nikhil Sharma,[†] Matthew S. Lamm,[†,§] Congqi Yan,[†] Radhika P. Nagarkar,[‡,∥] Joel P. Schneider,[‡,#] and Darrin J. Pochan[†,*]

[†]Department of Materials Science and Engineering, 201 DuPont Hall, University of Delaware, Newark, Delaware 19716, [‡]Department of Chemistry and Biochemistry, University of Delaware, Newark, Delaware 19716, [§]Current address: Merck Research Laboratories, Summit, NJ 07901, [∥]Current address: Glaxosmithkline Biopharm R&D, 709 Swedeland Road, King of Prussia, PA 19406, [#]Current address: Chemical Biology Laboratory, Center for Cancer Research, National Cancer Institute, Frederick, MD 21702-1201

ABSTRACT Self-assembly represents a robust and powerful paradigm for the bottom-up construction of nanostructures. Templated condensation of silica precursors on self-assembled nanoscale peptide fibrils with various surface functionalities can be used to mimic biosilicification. This template-defined approach toward biomineralization was utilized for the controlled fabrication of 3D hybrid nanostructures. The peptides MAX1 and MAX8 used herein form networks consisting of interconnected, self-assembled β-sheet fibrils. We report a study on the structure–property relationship of self-assembled peptide hydrogels where mineralization of individual fibrils through sol–gel chemistry was achieved. The nanostructure and consequent mechanical characteristics of these hybrid networks can be modulated by changing the stoichiometric parameters of the sol–gel process. The physical characterization of the hybrid networks *via* electron microscopy and small-angle scattering is detailed and correlated with changes in the network mechanical behavior. The resultant high fidelity templating process suggests that the peptide substrate can be used to template the coating of other functional inorganic materials.

KEYWORDS: self-assembly · peptide · template · sol–gel · hybrid materials

Nature is replete with mechanisms that co-assemble hard and soft materials, and these mechanisms have inspired multidisciplinary research at the threshold where biology meets chemistry.[1] Widely studied cases include the intricately patterned silica shell of marine organisms such as diatoms.[2] The complex silica motifs in such organisms highlight the importance of organic components as elements that intimately direct the uptake and organization of inorganic matter.[3,4] Prominent examples include long-chain polyamines in diatom shells and silicateins (silica proteins) in marine sponges.[5–7] Biologically generated silica is templated on such proteins from precursors such as orthosilicic acid, $Si(OH)_4$ present in ocean water.[8] Numerous strategies have been designed wherein organic templates such as polymers,[9,10] polymer–peptide hybrids,[11,12] block co-polypeptides,[13] self-assembling peptides,[14–16] and cationic peptide amphiphiles[17] were used to catalyze the sol–gel condensation of silica and other inorganic precursors. Templated sol–gel processes yield hybrid materials with diverse morphologies, and factors such as temperature, concentration, and pH of the reaction medium have substantial effects on the resultant shapes.[18] A unique dynamic templating paradigm has also been reported where template growth and inorganic deposition may proceed synergistically to form nanotubes of uniform dimensions.[19] In the studies presented herein, we used sol–gel chemistry to create well-defined silica shells around the fibrillar nanostructure of self-assembled peptide hydrogels. This procedure enables convenient control over the thickness of the silica shell around the peptide fibril, allowing definitive control over the shear modulus of the resulting hybrid networks. The silica coating bore a remarkable fidelity to the self-assembled peptide template, producing self-supporting monoliths with porosity spanning the nanoscale through mesoscale. In this paper, we detail the physical characterization of the peptide core–inorganic shell hybrid network and present rheological characterization of the networks highlighting the tunability of the shear modulus *via* the inorganic precursor concentration.

RESULTS AND DISCUSSION

Figure 1a shows a schematic outlining the self-assembly pathway of the MAX8 peptide. The 20 amino acid peptide ($VKVKVKVK^{D}P^{L}PTKVEVKVKV\text{-}NH_2$) has an overall positive charge at pH 7, due to its charged lysine residues, and adopts a random coil conformation when dissolved in

*Address correspondence to pochan@udel.edu.

Received for review September 14, 2009 and accepted December 4, 2009.

Published online December 22, 2009.
10.1021/nn901226h

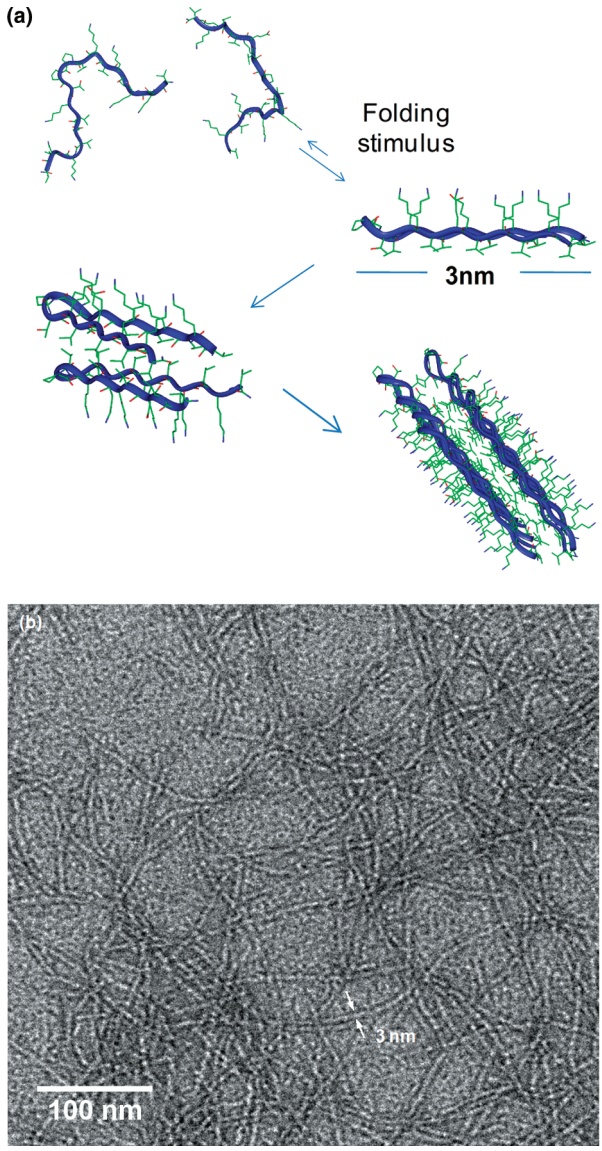

Figure 1. (a) Schematic for self-assembly of MAX8 peptide. (b) Transmission electron microscopy (TEM) image of negatively stained MAX8 fibrils with monodisperse 3 nm diameter.

deionized (DI) water. This peptide adopts a β-hairpin conformation *via* addition of an external stimulus. This intramolecular folding is analogous to the folding process that similar peptides that we have studied undergo with an increase in ionic strength,[20] pH,[21] temperature,[22] or light.[23] The intramolecular folding of MAX8 yields a facially amphiphilic β-hairpin with hydrophobic valine side chains and hydrophilic lysine side chains presented on opposite faces of the hairpin. This intramolecular folding is followed by intermolecular interactions through facial hydrophobic associations to form β-sheet bilayers, as shown in Figure 1a. Hydrogen bonding lateral to the peptide backbone and side chain hydrophobic contacts[24] among bilayers gives rise to the formation of fibrils. The fibrils have a high density of lysine groups exposed on the exterior surface as a result of self-assembly in an aqueous medium. Physical entanglements and branching[25,26] of these fibrils yield a self-supporting hydrogel (shown in Figure S1, Supporting Information). Transmission electron microscopy (TEM) was conducted to investigate the nanostructure of MAX8. Figure 1b shows a TEM image of MAX8 peptide fibrils negatively stained with uranyl acetate. Entangled peptide fibrils are observed with a monodisperse width of 3 nm, corresponding to the width of the folded peptide in β-hairpin conformation. Such well-defined peptide-based nanoscale morphologies[25−27] represent ideal structures for the templated organization of continuous inorganic phases as well as nanoparticles.[28,29] Additionally, the ability to engineer a diverse range of highly specific functionalities,[30] which may also incorporate biological recognition, into the assembled architecture without altering the network structure makes these peptide-based systems particularly useful from a bottom-up fabrication perspective.

The presence of a high number of protonated lysine groups on the fibril surface was utilized for the sol−gel condensation of inorganic silica precursor into a silica layer around the fibrils. This template-defined silica organization on the peptide fibrils results in a core−shell hybrid network with enhanced mechanical characteristics. Briefly, TMOS (or TEOS) was used as a silica precursor that generates orthosilicic acid, $Si(OH)_4$, when added to the preassembled hydrogel. It has been demonstrated that mono- and polyamines have the ability to catalyze the hydrolysis of organosilicates at circumneutral pH.[31,32] At around pH 7, silicic acid begins to dissociate into its silicate anion, $[SiO(OH)_3]^-$, with an increasing concentration toward higher pH values.[33] The electrostatic interaction between the positively charged lysine side chains and the various negatively charged anionic forms of dissociated silicic acid causes an increase in the local concentration of silicate anions in the vicinity of the fibril surface.[19] The lysine groups exposed on the fibril surface possibly also act as a catalytic site for the condensation of the silicate anions, and amine-catalyzed sol−gel polycondensation has been reported previously.[9,10,17,19] Polycondensation of the silicic acid results in uniform silica formation on the peptide fibril surface. TEM was conducted to characterize the structure of the silicified fibrils. Figure 2a shows a bright field TEM image of the silica-coated peptide fibrils. The composition of this shell was determined by a combination of X-ray energy-dispersive spectroscopy (data not shown), Fourier transform infrared spectroscopy (Figure S2, Supporting Information), and high-resolution TEM to be amorphous silica. Importantly, instances of nontemplated silica growth were not found, indicating that the growth of silica takes place with a high fidelity for the peptide template. Fairly monodisperse widths were observed for any sample with a constant molar ratio of peptide to precursor. Cryogenic scanning electron microscopy (cryo-SEM) was con-

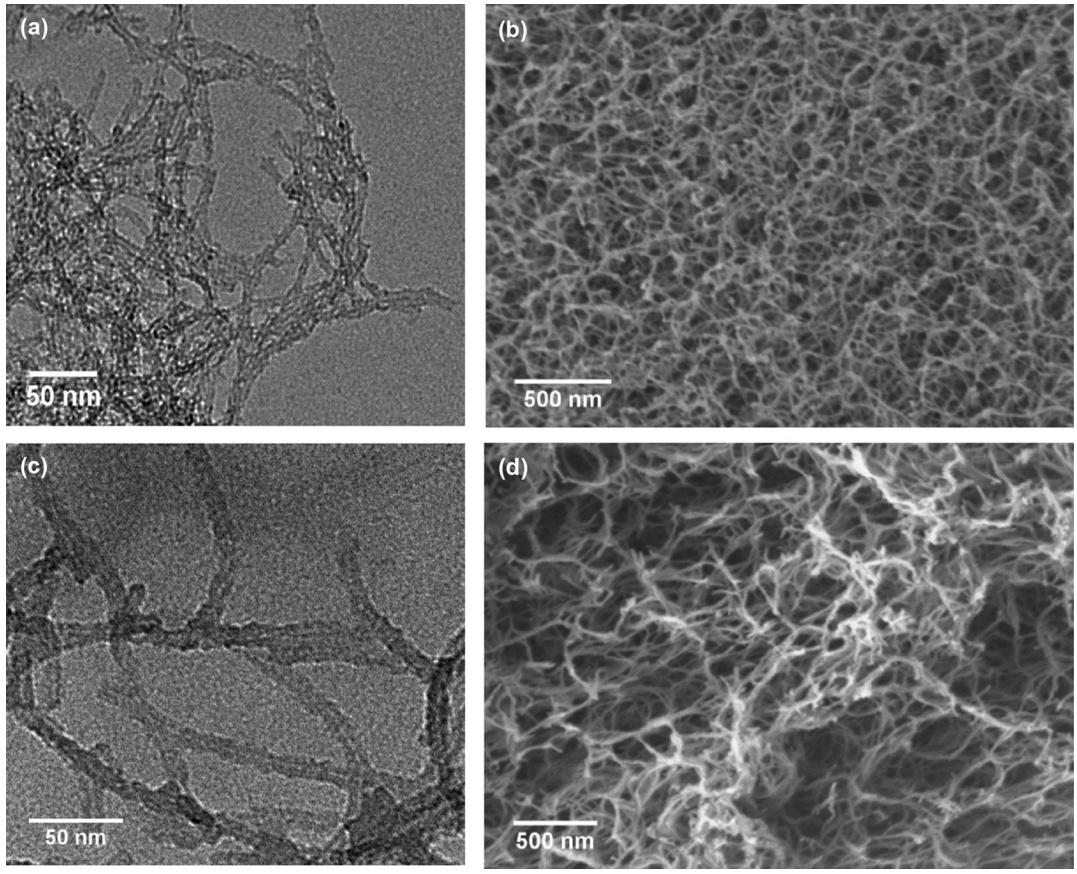

Figure 2. (a) TEM image of silica-coated MAX8 peptide fibrils showing dark silica shell encasing a light core of the peptide fibrils. (b) Cryo-SEM image silicified MAX8 fibrils. (c) TEM image of silicified MAX1 fibrils. (d) SEM image of silicified MAX1 fibrils showing high porosity and available void space. Samples were prepared for electron microscopy after 1 h of initial addition of the silica precursor to the hydrogel.

ducted to image the silicified peptide fibril network *in situ*. A cryo-SEM image of the silicified network is shown in Figure 2b. The image reveals a dense network of silicified peptide fibrils. As with TEM, a high fidelity of the precursor for the peptide fibrils is observed and the silica appears to preferentially coat the peptide fibrils. Dark regions on the micrograph correspond to void spaces, indicating the highly porous nature of the network. An analogous product was also observed with a similar peptide hydrogel MAX1 (VKVKVKVKV^{D}-P^{L}PTKVKVKVKV-NH_2)[21] tetraethyl orthosilicate (TEOS, silica precursor) system at pH 9. Figure 2c shows a TEM image of the dried silicified MAX1 fibrils. As with the MAX8−TMOS system, a uniform coating of silica is formed preferentially around the peptide fibrils. TEM imaging reveals the presence of a dark silica shell, due to the higher electron density of silica, encasing a lighter core of peptide fibrils. SEM imaging of the same sample (shown in Figure 2d) reveals a highly porous network with a large amount of void space. The surface area was measured by nitrogen absorption (BET analysis) to be ~230 m^2/g. The high surface area of these macroscale structures, comparable to nanoparticulate systems, may be utilized for impregnation with polymeric materials toward the aim of constructing hybrid interpenetrating networks.

Small-angle X-ray scattering (SAXS) and small-angle neutron scattering (SANS) were utilized to globally quantify changes in the local structure of silicified MAX1 (*via* TEOS) and silicified MAX8 (*via* TMOS) samples with varying silica precursor amounts. Figure 3 shows scattering curves for the hybrid networks, where scattering intensity $I(q)$ is plotted as a function of the scattering wave vector q ($Å^{-1}$). As the architecture of the silicified fibrils is composed of cylinder-like fibrils coated with silica, a core−shell cylinder form factor model was chosen to fit the SAXS and SANS data.[34] The modification of the contrast term allowed application of the same form factor model for SAXS and SANS data analysis.[35] Detailed information on scattering length densities utilized can be found in the Supporting Information. Experimental data fit well with the model except for the low-q regime (large length scales), where scattering contributions from longer range network structure become significant. Figure 3a compares SAXS data obtained from 0.5 wt % MAX1 gels with 0.04, 0.13, 0.21, and 0.41 M TEOS concentrations. The corresponding thicknesses extracted from the fits are 6.0, 12.3, 20.0,

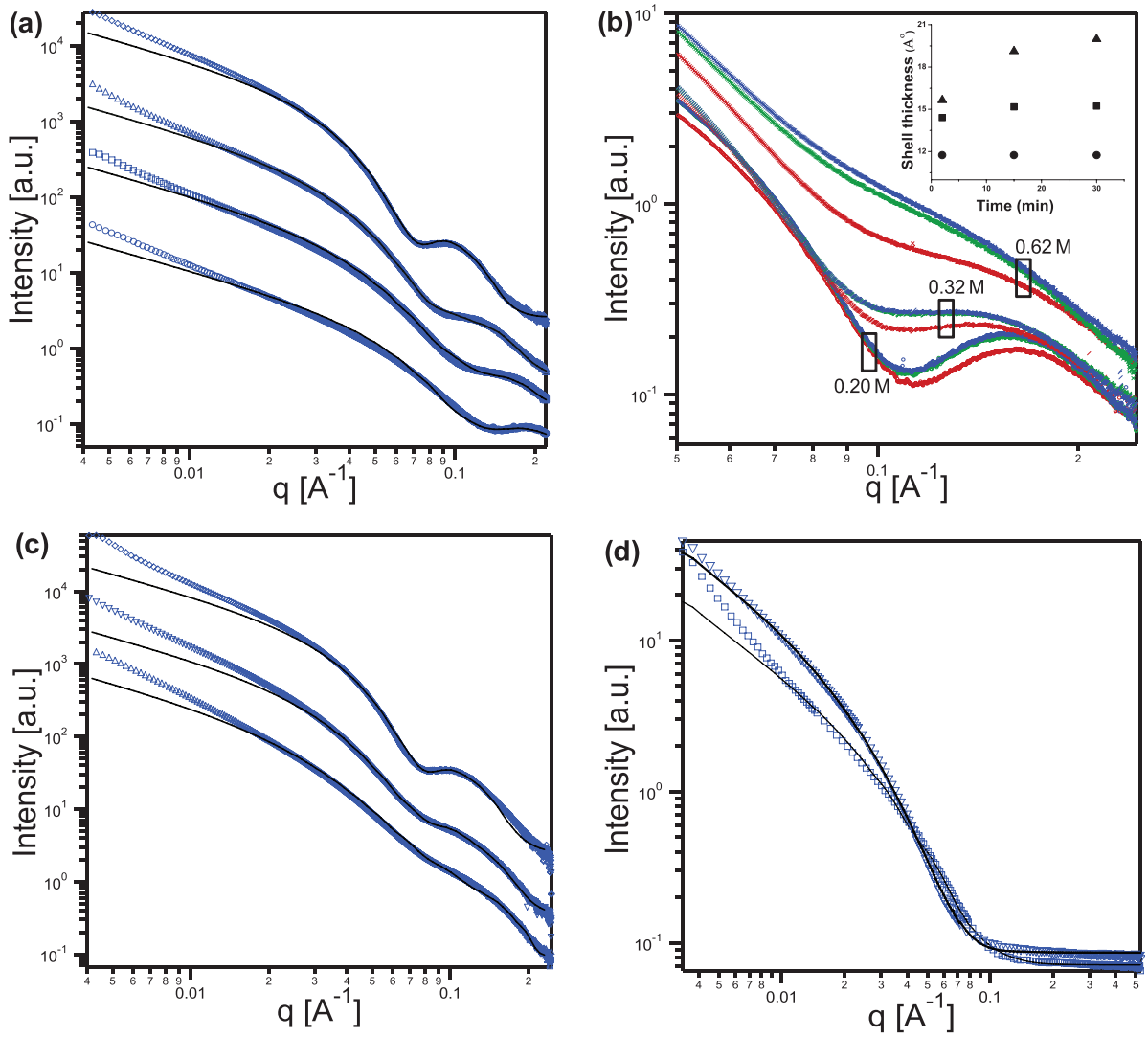

Figure 3. (a) Polydisperse core−shell cylinder model fits on SAXS curves of 0.5 wt % MAX1 samples with 0.04 M (○), 0.13 M (□), 0.21 M (△), 0.40 M (◇) TEOS. (b) SAXS data of kinetic series for 0.5 wt % MAX8 samples; scattering curves are grouped by boxes and represent 0.20 M (○) at 2 (red), 15 (green), and 30 (blue) min; 0.32 M(/)TMOS at 2 (red), 15 (green), and 30 (blue) min; and 0.62 M (X) at 2 (red), 15 (green), and 30 (blue) min; the inset plots radial shell thickness values (Å) observed with polydisperse core−shell cylinder fits as a function of time, and the symbols represent evolution of silica shell thicknesses for (●) 0.20 M, (■) 0.32 M, and (▲) 0.62 M TMOS in 0.5 wt % MAX8 hydrogel. (c) Polydisperse core−shell cylinder model fits on SAXS curves of 0.62 M TMOS in 0.5 wt % (△), 0.75 wt % (▽), and 1 wt % (◇) MAX8 samples. (d) Polydisperse core−shell cylinder model fits on SANS curves of 0.5 wt % MAX8 samples with 0.20 M (□) and 0.62 M (▽) TMOS.

and 30.4 Å, respectively. This is also manifested by the movement of the minima (in the high-q regime) toward lower q with increasing precursor amount, corresponding to the increase in overall scatterer diameter (in accordance with $J_1(qR_c) = 0$ for cylindrical particles, where J_1 is the first-order Bessel function of the radial cross section R_c).[34−37]

The temporal evolution of the silica shell, made possible due to the extremely high flux of the synchrotron source, was probed in a kinetic series where SAXS data were collected at periodic intervals of time. Time lapse SAXS data for 0.5 wt % MAX8 gels with 0.20, 0.32, and 0.62 M TMOS collected after 2, 15, and 30 min are shown in Figure 3b. The inset in Figure 3b shows a plot of shell thickness values extracted from fits as a function of time. The data show that the reaction rate is rapid, as clear changes are observed between 2 and 15 min with near identical scattering behavior at 15 and 30 min. A lack of clear form factor scattering was observed in the case where higher precursor amounts (0.32 and 0.62 M) were used due to increasing polydispersity in scatterer dimensions. In Figure 3c, TMOS concentration was held constant at 0.62 M and MAX8 hydrogels of 0.5, 0.75, and 1 wt % concentration were utilized. Remarkably, high fidelity templating, manifested by an increase in cylindrical form factor definition, is observed for the 1 wt % compared to 0.5 and 0.75 wt % hydrogel. As the concentration of the lysine groups increases (on increasing peptide concentration from 0.5 to 1 wt %) and approaches the concentration

of the precursor, the silica condensation again bears a high fidelity to the fibril template, evident from the reappearance of the minima in the low-q regime. Thus, the relative molar ratio of available lysine groups (peptide concentration) to precursor plays an important role in defining the local structure of the silicified peptide networks. Figure 3d displays SANS curves and polydisperse core−shell cylinder models for 0.5 wt % MAX8 hydrogels with 0.2 and 0.62 M TMOS. Inner radii (peptide fibril radii) extracted from the fit are 12.3 and 15.0 Å, respectively, and these match well with the diameters measured from TEM images and the theoretical width of 30 Å (Figure 1). As with SAXS, the corresponding silica shell thickness values were found to be 10.4 and 22.9 Å, representing a noteworthy change in the silica shell thickness. The small difference in inner radii for the two samples is marginal compared to the remarkable increase in outer radii for the sample with the higher precursor content. Hence, X-ray and neutron scattering results quantifiably validate the increase in silica shell thickness with increasing precursor amount.

Oscillatory rheology was conducted to track the evolution of the viscoelastic properties of the silicified fibril network. Examples of rheological measurements on a polymer−silica nanocomposite[38] and silica gels obtained by acid hydrolysis of an organosilicate in alcohol[39] have been reported previously. In our system, changing the stoichiometric parameters of the sol−gel process was observed to have a dramatic effect on the shear modulus of the resultant network. This dependence was studied by increasing the concentration of the precursor in two sets of hydrogel samples at different peptide concentrations; that is, increasing amounts of silica precursor were added to a fixed volume of 0.5 or 0.75 wt % hydrogel to produce increasingly stiffer silicified networks. Synthesis parameters and observed shear modulus values for the studied samples are outlined in Table 1. Shear moduli values (G') for the samples are plotted as a function of time in Figure 4. Figure 4a,b shows time sweep graphs for a preassembled 0.5 and 0.75 wt % hydrogel, respectively, and the silicified networks produced by adding increasing amounts of TMOS to the hydrogels. Shear modulus values in Table 1 are reported at 30 min after initiation of the sol−gel reaction. Dynamic frequency sweep data for the samples are shown in Figure S3 (Supporting Information). A comparison of the shear moduli of the studied samples shows that networks with stiffness values ranging from ~3 to 95 kPa can be produced by coating the peptide fibrils with silica. Samples with increasing TMOS contents, namely, $S^{0.5}_{0.2}$, $S^{0.5}_{0.3}$, and $S^{0.5}_{0.6}$, resulted in substrates with 9200, 2700, and 94 000 Pa G' values. A similar trend of increasing rigidity with increasing precursor concentration was also observed with 0.75 wt % hydrogel samples, $S^{0.75}_{0.2}$, $S^{0.75}_{0.3}$, and $S^{0.75}_{0.6}$, that resulted in networks with G' values of 3300, 10 400, and 14 200 Pa. A comparison of the moduli of samples

TABLE 1. Sample Designations,[a,b] Sol−Gel Processing Parameters, and Shear Moduli Values after 30 Minutes

sample designation S^y_x	MAX8 volume (μL)	TMOS volume (μL); concentration (M)	shear modulus, G' (Pa)
$S^{0.5}_0$	100	0; 0	~280
$S^{0.5}_{0.2}$	100	3; 0.20	~9200
$S^{0.5}_{0.3}$	100	5; 0.32	~27000
$S^{0.5}_{0.6}$	100	10; 0.62	~94000
$S^{0.75}_0$	100	0; 0	~800
$S^{0.75}_{0.2}$	100	3; 0.20	~3300
$S^{0.75}_{0.3}$	100	5; 0.32	~10400
$S^{0.75}_{0.6}$	100	10; 0.62	~14200

control designation C_x	solution volume (μL)	TMOS volume (μL); concentration (M)	shear modulus, G' (Pa)
$C_{0.2}$	100	3; 0.20	~80
$C_{0.6}$	100	10; 0.62	~5000

[a] S^y_x; x = tetramethyl orthosilicate concentration (TMOS) in hydrogel, y = wt % MAX8 hydrogel. [b] C_x; x = tetramethyl orthosilicate concentration (TMOS) in buffer without peptide.

$S^{0.5}_{0.2}$ and $S^{0.75}_{0.2}$, $S^{0.5}_{0.3}$ and $S^{0.75}_{0.3}$, or $S^{0.5}_{0.6}$ and $S^{0.75}_{0.6}$ shows that the modulus of the silicified network with the lower peptide concentration is higher. This is observed despite an opposite trend in moduli values of neat peptide hydrogel networks $S^{0.5}_0$ and $S^{0.75}_0$; that is, hydrogels with higher peptide concentration yield stiffer networks. This is because hydrogels prepared at higher peptide concentrations possess a higher number of available lysine groups available for reaction with the silica precursor. The silica precursor is therefore distributed over a larger number of fibrils, and this leads to an overall decrease in the thickness of the silica shell around each fibril, resulting in a network with a lower modulus. This is supported by comparison of radial shell thickness values obtained from the polydisperse core−shell cylinder model fits, as a function of MAX8 peptide concentration at constant TMOS concentration as shown in Table S3 (Supporting Information).

MAX8 hydrogel exhibits shear thinning characteristics, allowing the gel to flow freely like a solution under the influence of large shear forces, similar to those exerted on the contents of a syringe during injection.[40] Upon removal of the shear forces, the hydrogel immediately recovers into a stiff hydrogel. However, as physical interactions also define the magnitude of the gel's mechanical strength, the elastic moduli of most physical hydrogel systems are limited to low values of ~2 kPa. Coating the peptide fibrils with a thin layer of silica enhances the mechanical properties of the network by stiffening individual fibrils and reinforcing the entanglements, resulting in an increase in the rigidity of the network. As the added precursor amount is increased, keeping the hydrogel volume constant, the thickness of the resultant silica coating on the peptide fibril increases. A convenient way to describe the stiffened silicified fibrils is to approximate the networks as densely

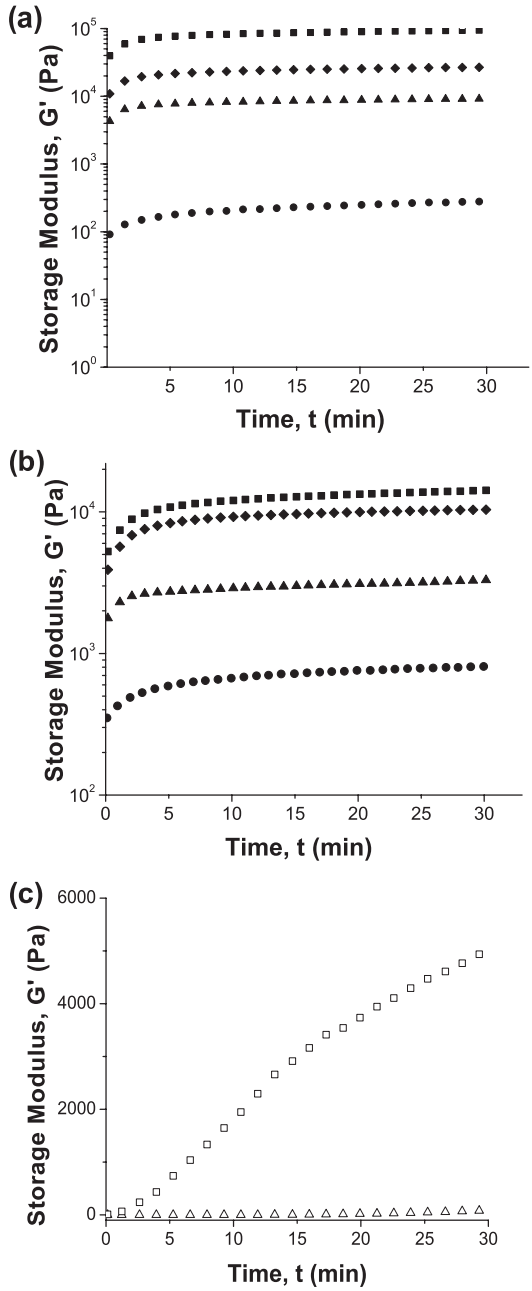

Figure 4. Oscillatory rheology time sweep curves for (a) 0.5 wt % and (b) 0.75 wt % preassembled MAX8−TMOS silicified peptide networks: (●) 0 M, (▲) 0.20 M (◆), 0.32 M, (■) 0.62 M in 0.5 wt % MAX8 hydrogel; (c) controls; (△) 0.20 M, (□) 0. 62 M TMOS in solution without peptide.

cross-linked meshes of semiflexible chains. Persistence lengths calculated for these samples using Mackintosh theory[41,42] assuming a constant network mesh size (as mesh size remains relatively constant with change in radial shell thickness) are 234, 410, and 765 nm. Frequency sweep data and the equation used for the calculation of persistence lengths are given in the Supporting Information. The increase in the persistence length on increasing precursor concentration as well as the reinforcement of physical cross-link junctions with a silica coating causes the dramatic increase in modulus. Importantly, the increase in modulus upon silicification is not simply a result of aggregation typically obtained in the sol−gel process,[43,44] as control silica gels prepared in the absence of the peptide template produced weak networks. Controls ($C_{0.2}$ and $C_{0.6}$, Table 1) prepared by adding TMOS to buffer alone produced networks with low moduli of up to 5 kPa (Figure 4c). Thus, the presence of the underlying peptide template during silicification is essential to achieving the high moduli that have been observed. Such enhancement in mechanical characteristics is most notably observed in biologically produced hybrids such as the nanostructured nacre of abalone shell.[45] Correlating rheology, SAXS and SANS results demonstrate that an increase in the silica shell thickness around individual peptide fibrils as well as a local stiffening in individual fibrils upon addition of the precursor accounts for the remarkable increase in elastic modulus of the network. Precursor amount thus constitutes a convenient and effective parameter by which the network rigidity may be tuned to a desired value by changing the silica layer thickness around the peptide fibrils.

CONCLUSIONS

In conclusion, we have described a simple procedure for creating hierarchically ordered, silica−peptide hybrid networks through sol−gel processing of peptide fibrils. When dried, monoliths possessing high surface areas can be produced where the interconnected network structure is preserved. The ability to systematically tune the shear modulus of the hybrid networks in a broad range of stiffness values simply by changing peptide to precursor ratio is a key advantage of this system. Self-assembling peptides such as MAX1 and MAX8 offer various opportunities to direct templating processes. The method described herein is not limited to producing nanostructured silica, and modularity afforded by the sol−gel process makes the process translatable to constructing hybrids of, for example, titania or other photocatalytically active materials. Experiments focused on the deployment of these materials as tissue engineering scaffolds are underway where a highly porous yet stiff scaffold is required. Tunable matrix elasticity and benign reaction conditions are other features that render this process amenable for biomaterial construction. The tunable modulus feature may also be utilized to create continuous reinforcement phases of tunable stiffness that may then be impregnated with other polymeric systems to produce interpenetrating, multifunctional microcomposites. Efforts toward the construction of such hierarchical composites are underway, and it is expected that composites containing these hybrid reinforcements would exhibit mechanical behavior significantly different from composites containing discrete particle fillers.

MATERIALS AND METHODS

Peptide Synthesis and Hydrogel Preparation: Details for MAX1 and MAX8 peptide synthesis have been reported previously.[21,40] MAX8 peptide hydrogel was prepared by first dissolving the peptide in DI water containing 10 mM HEPES buffer at pH 7.4. Self-assembly was initiated by the addition of an equal volume of DMEM cell culture medium (161 mM ionic strength from salts buffered to pH 7.4 with HEPES). MAX1 peptide hydrogel was prepared by dissolving the peptide in DI water. Self-assembly was initiated by the addition of an equal volume of borate buffer (250 mM borate, 20 mM NaCl) at pH9.

Sol−Gel Processing of Peptide Fibrils: Silicified networks were prepared by the direct addition of desired volume of TMOS to the preassembled MAX8 hydrogel (as shown in Table 1). Samples were vortexed for 20 s to allow the homogeneous distribution of the precursor. MAX1 samples were prepared by following the same procedure with the addition of TEOS to the preassembled MAX1 hydrogel. For characterization, the samples were aged in the vial for 1 h at ambient conditions after the initial addition of the precursor to the hydrogel unless otherwise stated.

Transmission Electron Microscopy: Five hundred microliters of DI water was added to a ~100 μL of sample, followed by probe sonication for 3 min. Five microliter solutions were applied to carbon-coated grids, and excess water was blotted away with filter paper. The grids were left to dry in ambient conditions for ~2 h. TEM was performed with JEOL JEM-2010f TEM equipped with X-ray energy-dispersive spectroscopy (XEDS) operating at 200 kV.

Scanning Electron Microscopy: SEM was conducted on the JEOL JSM-7400F SEM operating at voltages in the range 1 − 3 kV, in the standard (LEI) mode at working distances of 8 mm.

Cryogenic Scanning Electron Microscopy: Ten microliters of sample was loaded onto a freeze-fracture specimen carrier. The samples were frozen using a high pressure freezer. The sample holder was then transferred to a Gatan-Alto 2500 cryo-system where the sample was freeze fractured and subsequently sublimated for 5 min at −90 °C for the removal of ice crystals formed during the freezing process in liquid nitrogen. After the temperature was equilibrated back to −125 °C, the sample was sputtered with Au/Pd for 40 s. The sample was imaged on a Hitachi S-4700 SEM operating at 3 kV.

Small-Angle X-ray Scattering: SAXS experiments were performed at DND-CAT, Advanced Photon Source (APS), Argonne National Laboratory. Samples were prepared as described above. SAXS patterns at ambient temperatures were obtained from samples sandwiched between two Kapton sheets. The wavelength of the synchrotron source was 0.82 Å. Kapton tape was used as background and was subtracted from experimental intensity. The data were analyzed using the poly core−shell cylinder form factor model function. For kinetic series, data collection was initiated within 2 min of initial precursor addition.

Small-Angle Neutron Scattering: SANS experiments were conducted on the 30 m instrument on beamline NG7 at the National Center for Neutron Research, National Institute of Standards and Technology, Gaithersburg, MD. Samples were prepared in deuterated solutions to enhance contrast between solvent and sample. The neutron beam was monochromated to 6 Å using a velocity selector with a wavelength spread of $\Delta\lambda/\lambda = 0.15$. The scattered neutrons were detected by a 64 cm × 64 cm two-dimensional detector with three different sample-to-detector distances at 13.5, 4.5, and 1 m. These configurations allowed measurements to be performed between $0.004\ \text{Å}^{-1} < q < 0.5\ \text{Å}^{-1}$, in which q is the scattering vector defined as $q = 4\pi/\lambda \sin(\theta/2)$. The resulting spectra were corrected for background, detector efficiency non-uniformity, and empty cell scattering. The spectra were analyzed using the poly core−shell cylinder form factor model function which is available online (www.ncnr.nist.gov) at the National Center for Neutron Research.[34,35]

Oscillatory Rheology: Rheology experiments were conducted on TA Instruments AR2000 stress-controlled rheometer with 25 mm standard steel parallel plate geometry at 37 °C; 0.5 and 0.75 wt % hydrogel samples were mixed with the desired amount of TMOS, vortexed for 20 s, and immediately transferred to the rheometer with a micropipet. Data collection was initiated within 2 min of TMOS addition. Dynamic time sweep experiments were performed to monitor the storage (G') and loss (G'') modulus as a function of time (6 rad/s frequency, 0.2% strain) for 30 min. Shear modulus values were reported after approximately 30 min of the initial addition of the silica precursor to the preassembled hydrogels. Dynamic strain (0.1−10% strain, 6 rad/s frequency) and frequency (0.1−100 rad/s frequency, 0.2% strain) sweep experiments were performed on samples to establish the linear viscoelastic region and the frequency response of the samples.

Acknowledgment. A.A. and N.S. contributed equally to this work. We thank the College of Engineering, University of Delaware, for partial funding of W.M. Keck Electron Microscopy Facility, and C. Ni and F. Kriss, K. Czymmek and D. Powell at the University of Delaware. We thank S. Weigand for assistance with SAXS data acquisition, and J. Ilavsky for help with SAXS data analysis. X-ray scattering experiments were conducted with instruments maintained by Dupont−Northwestern−Dow Collaborative Access Team (DND-CAT) at the Advanced Photon Source at Argonne National Laboratories, USA. Use of the Advanced Photon Source at Argonne National Laboratory was supported by the U.S. Department of Energy, Office of Science, Office of Basic Energy Sciences, under Contract No. DE-AC02-06CH11357. Financial support from the National Health Institute R01 DE016386-01 and Army Research Laboratories (CMR CC-MT332157) is acknowledged. SANS experiments were partially supported by the UD Center for Neutron Science under 70NANB7H6178 from the National Institute of Standards and Technology (NIST), U.S. Department of Commerce. The statements, findings, conclusions, and recommendations are those of the authors and do not necessarily reflect the views of NIST or the U.S. Department of Commerce.

Supporting Information Available: Photograph of self-supporting structure of MAX8 hydrogel, FTIR spectrum or silica-coated MAX8 fibrils, dynamic frequency sweep of 0.5 wt % MAX8, persistence length calculations for silicified peptide networks at 0.5 wt % MAX8, and small-angle scattering length densities utilized for SAXS and SANS. This material is available free of charge *via* the Internet at http://pubs.acs.org.

REFERENCES AND NOTES

1. Dujardin, E.; Mann, S. Bio-inspired Materials Chemistry. *Adv. Mater.* **2002**, *14*, 775–788.
2. Kroger, N.; Deutzmann, R.; Sumper, M. Silica-Precipitating Peptides from Diatoms—The Chemical Structure of Silaffin-1A from *Cylindrotheca fusiformis*. *J. Biol. Chem.* **2001**, *276*, 26066–26070.
3. Hildebrand, M. Biological Processing of Nanostructured Silica in Diatoms. *Prog. Org. Coat.* **2003**, *47*, 256–266.
4. Halas, N. J. Nanoscience under Glass: The Versatile Chemistry of Silica Nanostructures. *ACS Nano* **2008**, *2*, 179–183.
5. Aizenberg, J.; Weaver, J. C.; Thanawala, M. S.; Sundar, V. C.; Morse, D. E.; Fratzl, P. Skeleton of *Euplectella* Sp.: Structural Hierarchy from the Nanoscale to the Macroscale. *Science* **2005**, *309*, 275–278.
6. Foo, C. W. P.; Huang, J.; Kaplan, D. L. Lessons from Seashells: Silica Mineralization *via* Protein Templating. *Trends Biotechnol.* **2004**, *22*, 577–585.
7. Cha, J. N.; Shimizu, K.; Zhou, Y.; Christiansen, S. C.; Chmelka, B. F.; Stucky, G. D.; Morse, D. E. Silicatein Filaments and Subunits from a Marine Sponge Direct the Polymerization of Silica and Silicones *In Vitro*. *Proc. Natl. Acad. Sci. U.S.A.* **1999**, *96*, 361–365.
8. Del Amo, Y.; Brzezinski, M. A. The Chemical form of Dissolved SI Taken up by Marine Diatoms. *J. Phycol.* **1999**, *35*, 1162–1170.
9. Mizutani, T.; Nagase, H.; Fujiwara, N.; Ogoshi, H. Silicic Acid Polymerization Catalyzed by Amines and Polyamines. *Bull. Chem. Soc. Jpn.* **1998**, *71*, 2017–2022.
10. Patwardhan, S. V.; Mukherjee, N.; Clarson, S. J. The Use of Poly-L-Lysine To Form Novel Silica Morphologies and the Role of Polypeptides in Biosilicification. *J. Inorg. Organomet. Polym.* **2001**, *11*, 193–198.

11. Kessel, S.; Thomas, A.; Borner, H. G. Mimicking Biosilicification: Programmed Coassembly of Peptide−Polymer Nanotapes and Silica. *Angew. Chem., Int. Ed.* **2007**, *46*, 9023–9026.
12. Kessel, S.; Borner, H. G. High Rate Silicification of Peptide−Polymer Assemblies toward Composite Nanotapes. *Macromol. Rapid Commun.* **2008**, *29*, 419–424.
13. Cha, J. N.; Stucky, G. D.; Morse, D. E.; Deming, T. J. Biomimetic Synthesis of Ordered Silica Structures Mediated by Block Copolypeptides. *Nature* **2000**, *403*, 289–292.
14. Meegan, J. E.; Aggeli, A.; Boden, N.; Brydson, R.; Brown, A. P.; Carrick, L.; Brough, A. R.; Hussain, A.; Ansell, R. J. Designed Self-Assembled Beta-Sheet Peptide Fibrils as Templates for Silica Nanotubes. *Adv. Funct. Mater.* **2004**, *14*, 31–37.
15. Holmstrom, S. C.; King, P. J. S.; Ryadnov, M. G.; Butler, M. F.; Mann, S.; Woolfson, D. N. Templating Silica Nanostructures on Rationally Designed Self-Assembled Peptide Fibers. *Langmuir* **2008**, *24*, 11778–11783.
16. Tomczak, M. M.; Glawe, D. D.; Drummy, L. F.; Lawrence, C. G.; Stone, M. O.; Perry, C. C.; Pochan, D. J.; Deming, T. J.; Naik, R. R. Polypeptide-Templated Synthesis of Hexagonal Silica Platelets. *J. Am. Chem. Soc.* **2005**, *127*, 12577–12582.
17. Yuwono, V. M.; Hartgerink, J. D. Peptide Amphiphile Nanofibers Template and Catalyze Silica Nanotube Formation. *Langmuir* **2007**, *23*, 5033–5038.
18. Yang, H.; Ozin, G. A.; Kresge, C. T. The Role of Defects in the Formation of Mesoporous Silica Fibers, Films, and Curved Shapes. *Adv. Mater.* **1998**, *10*, 883–887.
19. Pouget, E.; Dujardin, E.; Cavalier, A.; Moreac, A.; Valery, C.; Marchi-Artzner, V.; Weiss, T.; Renault, A.; Paternostre, M.; Artzner, F. Hierarchical Architectures by Synergy between Dynamical Template Self-Assembly and Biomineralization. *Nat. Mater.* **2007**, *6*, 434–439.
20. Ozbas, B.; Kretsinger, J.; Rajagopal, K.; Schneider, J. P.; Pochan, D. J. Salt-Triggered Peptide Folding and Consequent Self-Assembly into Hydrogels with Tunable Modulus. *Macromolecules* **2004**, *37*, 7331–7337.
21. Schneider, J. P.; Pochan, D. J.; Ozbas, B.; Rajagopal, K.; Pakstis, L.; Kretsinger, J. Responsive Hydrogels from the Intramolecular Folding and Self-Assembly of a Designed Peptide. *J. Am. Chem. Soc.* **2002**, *124*, 15030–15037.
22. Pochan, D. J.; Schneider, J. P.; Kretsinger, J.; Ozbas, B.; Rajagopal, K.; Haines, L. Thermally Reversible Hydrogels *via* Intramolecular Folding and Consequent Self- Assembly of a *De Novo* Designed Peptide. *J. Am. Chem. Soc.* **2003**, *125*, 11802–11803.
23. Haines, L. A.; Rajagopal, K.; Ozbas, B.; Salick, D. A.; Pochan, D. J.; Schneider, J. P. Light-Activated Hydrogel Formation *via* the Triggered Folding and Self-Assembly of a Designed Peptide. *J. Am. Chem. Soc.* **2005**, *127*, 17025–17029.
24. Rajagopal, K.; Ozbas, B.; Pochan, D. J.; Schneider, J. P. Probing the Importance of Lateral Hydrophobic Association in Self-Assembling Peptide Hydrogelators. *Eur. Biophys. J. Biophys. Lett.* **2006**, *35*, 162–169.
25. Ozbas, B.; Rajagopal, K.; Schneider, J. P.; Pochan, D. J. Semiflexible Chain Networks Formed *via* Self-Assembly of Beta-Hairpin Molecules. *Phys. Rev. Lett.* **2004**, 93.
26. Yucel, T.; Micklitsch, C. M.; Schneider, J. P.; Pochan, D. J. Direct Observation of Early- Time Hydrogelation in Beta-Hairpin Peptide Self-Assembly. *Macromolecules* **2008**, *41*, 5763–5772.
27. Lamm, M. S.; Rajagopal, K.; Schneider, J. P.; Pochan, D. J. Laminated Morphology of Nontwisting Beta-Sheet Fibrils Constructed *via* Peptide Self-Assembly. *J. Am. Chem. Soc.* **2005**, *127*, 16692–16700.
28. Lamm, M. S.; Sharma, N.; Rajagopal, K.; Beyer, F. L.; Schneider, J. P.; Pochan, D. J. Laterally Spaced Linear Nanoparticle Arrays Templated by Laminated Beta-Sheet Fibrils. *Adv. Mater.* **2008**, *20*, 447–451.
29. Sharma, N.; Top, A.; Kiick, K. L.; Pochan, D. J. One-Dimensional Gold Nanoparticle Arrays by Electrostatically Directed Organization Using Polypeptide Self-Assembly. *Angew. Chem., Int. Ed.* **2009**, *48*, 7078–7082.
30. Whaley, S. R.; English, D. S.; Hu, E. L.; Barbara, P. F.; Belcher, A. M. Selection of Peptides with Semiconductor Binding Specificity for Directed Nanocrystal Assembly. *Nature* **2000**, *405*, 665–668.
31. Delak, K. M.; Sahai, N. Amine-Catalyzed Biomimetic Hydrolysis and Condensation of Organosilicate. *Chem. Mater.* **2005**, *17*, 3221–3227.
32. Sudheendra, L.; Raju, A. R. Peptide-Induced Formation of Silica from Tetraethylorthosilicate at Near-Neutral pH. *Mater. Res. Bull.* **2002**, *37*, 151–159.
33. Thakur, P.; Singh, D. K.; Choppin, G. R. Polymerization Study of o-Si(OH)(4) and Complexation with Am(III), Eu(III) and Cm(III). *Inorg. Chim. Acta* **2007**, *360*, 3705–3711.
34. Pizzey, C. L.; Pomerantz, W. C.; Sung, B. J.; Yuwono, V. M.; Gellman, S. H.; Hartgerink, J. D.; Yethiraj, A.; Abbott, N. L. Characterization of Nanofibers Formed by Self-Assembly of Beta-Peptide Oligomers Using Small Angle X-ray Scattering. *J. Chem. Phys.* **2008**, *129*, 095103.
35. Kline, S. R. Reduction and Analysis of SANS and USANS Data Using IGOR Pro. *J. Appl. Crystallogr.* **2006**, *39*, 895–900.
36. Bang, J.; Jain, S. M.; Li, Z. B.; Lodge, T. P.; Pedersen, J. S.; Kesselman, E.; Talmon, Y. Sphere, Cylinder and Vesicle Nanoaggregates in Poly(styrene-*b*-isoprene) Diblock Copolymer Solutions. *Macromolecules* **2006**, *39*, 1199–1208.
37. Porod, G. Glatter, O. Kratky O. *Small Angle X-ray Scattering*; Academic Press: New York, 1982.
38. Pek, Y. S.; Wan, A. C. A.; Shekaran, A.; Zhuo, L.; Ying, J. Y. A Thixotropic Nanocomposite Gel for Three-Dimensional Cell Culture. *Nat. Nanotechnol.* **2008**, *3*, 671–675.
39. Dumas, J.; Baza, S.; Serughetti, J. Silica-Gels from the Alkoxide Method—Dependence of Shear Modulus on Concentration. *J. Mater. Sci. Lett.* **1986**, *5*, 478–480.
40. Haines-Butterick, L.; Rajagopal, K.; Branco, M.; Salick, D.; Rughani, R.; Pilarz, M.; Lamm, M. S.; Pochan, D. J.; Schneider, J. P. Controlling Hydrogelation Kinetics by Peptide Design for Three-Dimensional Encapsulation and Injectable Delivery of Cells. *Proc. Natl. Acad. Sci. U.S.A.* **2007**, *104*, 7791–7796.
41. Mackintosh, F. C.; Kas, J.; Janmey, P. A. Elasticity of Semiflexible Biopolymer Networks. *Phys. Rev. Lett.* **1995**, *75*, 4425–4428.
42. Branco, M. C.; Pochan, D. J.; Wagner, N. J.; Schneider, J. P. Macromolecular Diffusion and Release from Self-Assembled Beta-Hairpin Peptide Hydrogels. *Biomaterials* **2009**, *30*, 1339–1347.
43. Hench, L. L.; West, J. K. The Sol−Gel Process. *Chem. Rev.* **1990**, *90*, 33–72.
44. Coradin, T.; Lopez, P. J. Effect of Some Amino Acids and Peptides on Silicic Acid Polymerization. *ChemBioChem* **2003**, *4*, 251–259.
45. Sellinger, A.; Weiss, P. M.; Nguyen, A.; Lu, Y. F.; Assink, R. A.; Gong, W. L.; Brinker, C. J. Continuous Self-Assembly of Organic−Inorganic Nanocomposite Coatings That Mimic Nacre. *Nature* **1998**, *394*, 256–260.